Adsorption (2015) 21:107–123
DOI 10.1007/s10450-015-9654-z

Hydrogen recovery from off-gases with nitrogen-rich impurity by pressure swing adsorption using CaX and 5A zeolites

José A. Delgado · Vicente I. Agueda · María A. Uguina · José L. Sotelo · Pablo Brea

Received: 22 September 2014 / Revised: 17 December 2014 / Accepted: 12 January 2015 / Published online: 21 January 2015

Abstract Many studies in the literature about pressure swing adsorption (PSA) hydrogen purification deal with the recovery of hydrogen from off-gases where nitrogen concentration in the feed mixture is usually below 5 %. Practical examples of hydrogen-containing off-gases with higher nitrogen concentration are total hydrocarbon reforming off-gas, and coke oven gas. In this work, the separation performance of CaX and 5A zeolites in the hydrogen recovery from these gases by PSA is compared using a simulation tool called PSASIM. Reciprocal diffusion time constants and adsorption isotherms of nitrogen, methane and carbon monoxide in CaX zeolite measured experimentally are included. Simulations show that, with a feed pressure of 3 bar, CaX yields higher hydrogen recovery than 5A zeolite for the same product purity (above 99.7 %) with both feed gases. CaX removes nitrogen better than 5A zeolite, although it is worse for removing carbon monoxide and methane. The hydrogen recovery can be increased notably (from about 65 % to above 90 %) by including a rinse step in the PSA cycle while maintaining high hydrogen product purity.

Keywords Hydrogen purification · Pressure swing adsorption · Coke oven gas · Adsorption · Diffusion · Simulation · CaX zeolite

List of symbols

b	Adsorption affinity (Pa^{-1})
$b_{01,2}$	Parameters in Dual Langmuir model (Pa^{-1})
c	Adsorptive concentration in the gas phase (mol m^{-3})
C	Total gas concentration (mol m^{-3})
$c_{p,g}$	Gas heat capacity at constant pressure (J mol^{-1} K^{-1})
$c_{p,s}$	Adsorbent heat capacity (J kg^{-1} K^{-1})
$c_{p,w}$	Wall heat capacity (J kg^{-1} K^{-1})
$c_{v,g}$	Gas heat capacity at constant volume (J mol^{-1} K^{-1})
D_c	Micropore diffusivity (m^2 s^{-1})
D_L	Axial dispersion coefficient (m^2 s^{-1})
D_m	Molecular diffusivity (m^2 s^{-1})
E_{diff}	Activation energy of diffusion (kJ mol^{-1})
h_{sg}	Solid to gas heat transfer coefficient (W m^{-2} K^{-1})
h_w	Wall-gas heat transfer coefficient (W m^{-2} K^{-1})
K	Adsorption equilibrium Henry's law constant (m^{3gas} $m^{-3solid}$)
K_H	Adsorption equilibrium Henry's law constant (mol kg^{-1} Pa^{-1})
k_f	External mass transfer coefficient (m s^{-1})
k_g	Gas conductivity (W m^{-1} K^{-1})
k_{macro}	Combined mass transfer coefficient in the external film and the macropores (m s^{-1})
n	Adsorbed concentration (mol kg^{-1})
n	Number of components
N.S.	Normalized signal (area below the pulse is set to 1)
$n_{max1,2}$	Parameters in Dual Langmuir model (mol kg^{-1})
p	Adsorptive pressure (Pa)
P	Pressure (Pa)
Pr	Prandtl number
Q_{st}	Average isostericheat (J mol^{-1})
R	Gas constant (J mol^{-1} K^{-1})
r^2	Coefficient of determination

J. A. Delgado (✉) · V. I. Agueda · M. A. Uguina · J. L. Sotelo · P. Brea
Department of Chemical Engineering, Universidad Complutense de Madrid, 28040 Madrid, Spain
e-mail: jadeldob@ucm.es

r_c	Half diffusion length in micropores (m)
Re	Particle Reynolds number
R_p	Radius of adsorbent particle (m)
R_w	Column wall radius (m)
Sc	Schmidt number
T	Temperature (K)
t	Time (s)
u	Superficial velocity (m s^{-1})
U	Wall to surroundings heat transfer coefficient (W m^{-2} K^{-1})
x	Mole fraction in the adsorbed phase
y	Mole fraction in the gas phase
z	Axial coordinate (m)
$\Delta H_{1,2}$	Parameters in Dual Langmuir model (kJ mol^{-1})

Greek symbols

ε	Bed voidage fraction between adsorbent particles
ε_p	Particle porosity
λ	Axial heat dispersion coefficient (W m^{-1} K^{-1})
μ	Gas viscosity (Pa s)
π	Spreading pressure (N m^{-1})
ρ_g	Gas density (kg m^{-3})
ρ_p	Particle density (kg m^{-3})
ρ_w	Wall density (kg m^{-3})
τ	Tortuosity

1 Introduction

Production of hydrogen is becoming increasingly important nowadays. Recently the development of new hydrogen technologies has been the focus of international attention to increase energy and economic security. Hydrogen can be produced from different feed stocks, such as fossil resources (natural gas, oil refinery fractions and coal), or renewable resources (biomass and water with sunlight, wind, wave or hydro-power as sources of energy) (Riis et al. 2006).

Steam reforming of methane (SMR) is the most common hydrogen production method in commercial use today (Holladay et al. 2009). In this process, the main impurities that accompany hydrogen are carbon dioxide and carbon monoxide. Other alternatives are partial oxidation, auto thermal reforming of hydrocarbon fuels, and coal gasification (Besancon et al. 2009). When air is used as reactant in the process, like in total hydrocarbon reforming (Bakta 1999), or nitrogen is used as carrier gas (Besancon et al. 2009; Cormos et al. 2008), a large amount of nitrogen is added to the impurities that accompany hydrogen in the product gas.

Hydrogen can also be obtained from coke oven gas (COG), which results in the coking process in steel mills (Joseck et al. 2008). Major impurities mixed with hydrogen in COG are methane, nitrogen, carbon monoxide and carbon dioxide, where a typical concentration of nitrogen is about 10 % v/v.

Pressure swing adsorption (PSA) is one of the most used technologies for recovering hydrogen from off-gases (Yang 1997; Ruthven et al. 1994). In this unit, a hydrogen-containing gas mixture is passed to at least one of several adsorption beds at an elevated pressure, where the impurities are sequentially adsorbed in the bed by virtue of their different affinities towards the adsorbent or adsorbents used (Baksh ans Simo 2013). As hydrogen is the least adsorbed component, it passes through the bed and it is obtained with high purity in the outlet stream.

Different adsorbents in a layered configuration are commonly employed to improve the unit performance, where each adsorbent is intended for adsorbing some target impurities (Chlendi and Tondeur 1995; Beaver and Sircar 2010). In industrial PSA units, 5A zeolite is widely used to remove methane, carbon monoxide and nitrogen from hydrogen mixtures. Although pilot plant performance data are generally required for designing and optimizing PSA processes, realistic process simulation models can be used for screening process concepts and adsorbent materials, as well as for doing a tentative process design (Waldron and Sircar 2000). For this purpose, adsorption equilibrium data (adsorption isotherms of the main components in the gas mixture and adsorption heats), together with diffusion data are required (Lopes et al. 2010; Saha et al. 2010). This information must be incorporated into the simulation model to study the proposed process (Barg et al. 2000; Biswas et al. 2010; Dowling et al. 2012; Mofarahi and Shokroo 2013; Casas et al. 2013).

Many studies in the literature about PSA hydrogen purification are intended for the treatment of SMR off-gases, where nitrogen concentration in the feed mixture is usually below 5 % or negligible (Park et al. 2000; Sircar et al. 1999; Ribeiro et al. 2009; Lopes et al. 2011; Jang et al. 2011; Chen and Fair 2013). The studies dealing with higher nitrogen concentrations are scarcer. Due to the relatively low affinity of nitrogen to most adsorbents, its presence in the mixture increases the difficulty of obtaining high purity hydrogen by PSA.

Hydrogen recovery from coke oven gas (with 5.5–7.5 % nitrogen) by PSA has been studied experimentally by Ahn et al. (2001). Zhou et al. (2002) studied experimentally the recovery of hydrogen from simulated catalytic dry gas of refineries (60 % hydrogen, 30 % methane and 10 % nitrogen) by a novel PSA cycle. Tomita et al. (1987) studied the hydrogen recovery by PSA from the product gas of a total hydrocarbon reforming process of residual oils, containing 27 % nitrogen.

In this work, the use of CaX zeolite for the recovery of hydrogen from mixtures containing high nitrogen concentration by PSA is studied. CaX zeolite has been chosen as

adsorbent because of its high affinity towards nitrogen (Ruthven et al. 1994; Lopes et al. 2010).

Although the application of CaX to hydrogen purification by PSA has been studied recently (Chou et al. 2013), and it has been proposed in patents (i.e. Baksh and Simo 2013), little information is available in the open literature about its application to hydrogen recovery from mixtures with high nitrogen content.

Two examples of feeds have been considered, a stream coming from a total hydrocarbon reforming process of residual oils (69.2 % H_2, 26.8 % N_2, 1.8 % CH_4, 2.2 % CO, Tomita et al. 1987), called THRG from now on, and coke oven gas (COG) with a typical composition (57.3 % H_2, 10.4 % N_2, 26.1 % CH_4, 6.2 % CO, Joseck et al. 2008). For THRG, it is assumed that other impurities like carbon dioxide have been removed previously with amine absorption (Tomita et al. 1987). For COG, it is also assumed that the concentrations of other impurities apart from nitrogen, carbon monoxide and methane in the gas treated with the zeolitic adsorbent are very low (Yang et al. 1997).

The objectives of this work are the following:

(1) To measure the reciprocal diffusion time constants of carbon monoxide, nitrogen and methane on CaX zeolite at temperatures between 25 and 65 °C.
(2) To measure the adsorption isotherms of hydrogen, carbon monoxide, nitrogen and methane on CaX zeolite at temperatures between 25 and 65 °C
(3) To compare the performance of CaX and 5A zeolites in the recovery of hydrogen by PSA from the mixtures described previously by simulation. For CaX, the required equilibrium and kinetic information has been obtained experimentally. For 5A zeolite, this information has been taken from the literature (Tomita et al. 1987).

2 Experimental

CaX zeolite was prepared by ion exchange from commercial NaX zeolite pellets, supplied by Union Carbide. The ion exchange was carried out three times in a microwave oven (Milestone 1200 MEGA) with aqueous $CaCl_2$ (1 M) at 353 K during 30 min each time, washing the solid with Milli-Q water after each exchange. The initial Ca^{2+} and Na^{+} concentrations in the NaX zeolite were 0.03 and 11.75 % w/w, respectively, measured by XRF. After the ion exchange, the Ca^{2+} and Na^{+} concentrations were 10.9 and 1.99 % w/w, respectively. The size of the crystals was determined by SEM (Delgado et al. 2014), with sizes ranging between about 2-4 microns. Table 1 shows the adsorbent properties.

All the gases in this study had purities higher than 99.99 % supplied by Praxair. The adsorption isotherms of the studied gases have been measured in a volumetric equipment (Micromeritics ASAP 2000). Prior to the experiments, the adsorbent was regenerated under vacuum overnight at 623 K.

Pulse experiments were performed with a column packed with CaX pellets, placed inside the temperature controlled oven of a gas chromatograph (Varian CP3800), equipped with a TCD detector. The flow rate of carrier gas is controlled with the mass flow rate controller of the chromatograph. Bed properties in the pulse experiments are shown in Table 2.

In each pulse experiment, a 50 µl loop filled with the studied gas is swept by the carrier gas, and the pulse response is registered by the TCD detector. Helium was used as carrier gas when nitrogen, methane, carbon monoxide are the adsorbates. Helium pulses were also recorded to measure the void volume and the global dispersion in the installation (including the dispersion caused by the detector), using nitrogen as carrier gas. Prior to the pulse experiments, the adsorbent was regenerated at 623 K overnight under helium flow.

3 Results and discussion

3.1 Measurement of reciprocal diffusion time constants in CaX

The reciprocal diffusion time constants (D_c/r_c^2) of nitrogen, methane and carbon monoxide in CaX zeolite have been measured from pulse experiments with a well-proven chromatographic method (Delgado et al. 2014). Although pulse experiments with hydrogen as adsorbate were also carried out, it was not possible to obtain reliable pulse responses with this gas because of the little sensitivity of the TCD detector towards hydrogen in hydrogen/helium mixtures. Fortunately, the reciprocal diffusion time constant of hydrogen is usually much higher than that of other gases because of its lower adsorption affinity (Lopes et al. 2010), and it can usually be assumed that this parameter is infinite for simulating a hydrogen purification PSA cycle, because its effect on performance results is negligible.

The chromatographic method has been explained in detail elsewhere (Delgado et al. 2014), so only a brief explanation is given here. Adsorption Henry's law constants are calculated from the first moment of pulse responses, taking into account the void volume in the installation, measured from helium pulses with nitrogen as carrier gas, considering helium as a non-adsorbing gas. Helium pulses are also used to model the effect of global dispersion in the installation on the pulse response, using a

Table 1 Properties of CaX zeolite pellets

Particle density (g cm^{-3})[a]	Pellet size (mm)	Particle porosity[a]	Average pore diameter (nm)[b]	BET surface (m^2 g^{-1})[b]
1.36	1.5	0.47	2.21	498

[a] Taken as the values measured experimentally by Hg porosimetry from the parent NaX zeolite (Delgado et al. 2014). Particle porosity is calculated considering the void volume estimated by Hg porosimetry only

[b] Measured by nitrogen porosimetry

Table 2 Bed properties in the pulse experiments

Bed length (cm)	Mass of pellets (g)	Porosity between particles	Bed diameter (cm)
2.55	0.669	0.642	0.83

plug-flow and tank-in-series model. A theoretical model based in conservation equations is used to extract the reciprocal diffusion time constants from the experimental pulse responses by non-linear regression. The effect of diffusion in pellet macropores is included in the theoretical model, so the measured value of D_c/r_c^2 corresponds to diffusion in CaX zeolite crystals.

The model is fitted simultaneously to a group of pulse responses for each adsorbate at constant temperature with different carrier gas flow rates, imposing the same value of D_c/r_c^2 for all the pulses in the group, and the fitting quality is evaluated with the coefficient of determination (r^2). The measured values of D_c/r_c^2 are presented in Table 3, together with the measured values of the adsorption Henry's law constant (K, in m^3_{gas} m^{-3}_{solid}). To express this constant in units of mol kg^{-1} Pa^{-1}, the following formula must be used (Delgado et al. 2014):

$$K_H = \frac{K(1-\varepsilon_p)}{\rho_p RT} \quad (1)$$

A comparison between the theoretical and experimental pulse responses is presented in Fig. 1.

It must be noted that the experimental pulse responses are not symmetrical (they are skewed). This is mainly due to the effect of the dispersion outside the bed on the pulse response (because of void volume in tubing and detector). Micropore diffusion control under linear conditions also contributes to the tailing of the pulse (Karger and Ruthven 1992). Chromatographic methods for diffusion measurements used in the literature usually neglect the effect of dispersion outside the adsorbent bed. A long bed is necessary to minimize the effect of dispersion outside the bed, which can lead to a very wide pulse whose maximum height differs little from the baseline. In our work, we have observed that dispersion outside the bed is quite important, and it has been measured experimentally using helium as non-adsorbing tracer. The model takes into account the effect of overall dispersion outside the bed with a plug-flow and tank-in-series model. Model details can be found elsewhere (Delgado et al. 2014).

Although all the graphs in this figure are apparently similar, the difference in the scales in both axes must be noted, particular for carbon monoxide. The good fitting quality of the complete pulse responses (including adsorption and desorption) is indicative of the physical significance of the measured diffusion parameters, as the reciprocal diffusion time constant is the only fitted parameter for each group of pulses at constant temperature. The reciprocal diffusion time constant is much lower for carbon monoxide than for methane, and the value for methane is lower than for nitrogen, which coincides with a much higher value of K for carbon monoxide, followed by methane and nitrogen. This indicates that the diffusion in the crystal micropores is greatly influenced by the residence time in the adsorption sites, which depends on the adsorption affinity of the adsorbate, as it was observed for NaX zeolite (Delgado et al. 2014).

The activation energy of diffusion (E_{diff} in Table 3) is also consistent with this hypothesis, being much higher for carbon monoxide than for methane and nitrogen. The higher affinity of carbon monoxide is due to the interaction of its dipole and quadrupole moment with calcium ions, and the higher affinity of methane with respect to nitrogen is due to its higher polarizability.

The values of D_c/r_c^2 at 298 K of the studied gases are of the same order of magnitude as the ones measured by Lopes et al. (2010) in CaX extrudates with crystals of similar size at a close temperature (303 K): 0.035 s^{-1} for N_2, 0.005 s^{-1} for CO and 0.02 s^{-1} for CH_4. The different Ca^{2+} concentration in the CaX sample (7.6 % against 10.9 % in this work) seems to have little effect on the diffusion of the studied gases. The value of K_H for CO in CaX at 298 K obtained in this work (1.7×10^{-4} mol kg^{-1} Pa^{-1}) is also of the same order of magnitude as the one reported by Lopes et al. (2010) (1.17×10^{-4} mol kg^{-1} Pa^{-1}).

The effect of exchanging sodium by calcium in NaX zeolite on adsorption and diffusion parameters is analysed in Table 4, where a comparison between the values of K and D_c/r_c^2 for NaX (Delgado et al. 2014) and CaX zeolite is presented. It is observed that K and the activation energy of

Table 3 Experimental conditions for the pulse experiments with nitrogen, carbon monoxide, and methane in CaX pellets, and measured adsorption and diffusion parameters

Gas	Q (10^{-6} m^3 s^{-1})	T (K)	K	D_c/r_c^2 (s^{-1})	E_{diff} (kJ mol^{-1})	r^2
N_2	0.50	298	66.7 ± [a]0.4	0.048 ± [b]8 × 10^{-4}	24.8 ± [a]0.3	0.997
N_2	1.01	298	65.8 ± 0.4	0.048 ± 8 × 10^{-4}	24.8 ± 0.3	0.997
N_2	1.50	298	67.8 ± 0.4	0.048 ± 8 × 10^{-4}	24.8 ± 0.3	0.997
N_2	1.92	298	67.3 ± 0.4	0.048 ± 8 × 10^{-4}	24.8 ± 0.3	0.997
N_2	0.51	313	51.2 ± 1.3	0.081 ± 1 × 10^{-3}	24.8 ± 0.3	0.998
N_2	0.99	313	46.3 ± 1.3	0.081 ± 1 × 10^{-3}	24.8 ± 0.3	0.998
N_2	1.50	313	51.3 ± 1.3	0.081 ± 1 × 10^{-3}	24.8 ± 0.3	0.998
N_2	1.85	313	47.5 ± 1.3	0.081 ± 1 × 10^{-3}	24.8 ± 0.3	0.998
N_2	0.52	338	23.0 ± 0.3	0.158 ± 3 × 10^{-3}	24.8 ± 0.3	0.998
N_2	1.02	338	22.4 ± 0.3	0.158 ± 3 × 10^{-3}	24.8 ± 0.3	0.998
N_2	1.52	338	23.3 ± 0.3	0.158 ± 3 × 10^{-3}	24.8 ± 0.3	0.998
N_2	1.98	338	23.8 ± 0.3	0.158 ± 3 × 10^{-3}	24.8 ± 0.3	0.998
CO	0.50	298	1,037 ± 32	0.0029 ± 6 × 10^{-5}	41.4 ± 0.2	0.996
CO	0.99	298	1,043 ± 32	0.0029 ± 6 × 10^{-5}	41.4 ± 0.2	0.996
CO	1.50	298	1,137 ± 32	0.0029 ± 6 × 10^{-5}	41.4 ± 0.2	0.996
CO	1.94	298	1,163 ± 32	0.0029 ± 6 × 10^{-5}	41.4 ± 0.2	0.996
CO	0.48	313	584 ± 20	0.0066 ± 8 × 10^{-5}	41.4 ± 0.2	0.998
CO	0.98	313	642 ± 20	0.0066 ± 8 × 10^{-5}	41.4 ± 0.2	0.998
CO	1.50	313	551 ± 20	0.0066 ± 8 × 10^{-5}	41.4 ± 0.2	0.998
CO	2.06	313	569 ± 20	0.0066 ± 8 × 10^{-5}	41.4 ± 0.2	0.998
CO	0.48	338	200 ± 7	0.021 ± 2 × 10^{-4}	41.4 ± 0.2	0.999
CO	1.00	338	225 ± 7	0.021 ± 2 × 10^{-4}	41.4 ± 0.2	0.999
CO	1.50	338	228 ± 7	0.021 ± 2 × 10^{-4}	41.4 ± 0.2	0.999
CO	2.00	338	230 ± 7	0.021 ± 2 × 10^{-4}	41.4 ± 0.2	0.999
CH_4	0.52	298	86.5 ± 1	0.038 ± 7 × 10^{-4}	24.9 ± 0.2	0.997
CH_4	1.01	298	82.3 ± 1	0.038 ± 7 × 10^{-4}	24.9 ± 0.2	0.997
CH_4	1.49	298	86.3 ± 1	0.038 ± 7 × 10^{-4}	24.9 ± 0.2	0.997
CH_4	2.01	298	84.2 ± 1	0.038 ± 7 × 10^{-4}	24.9 ± 0.2	0.997
CH_4	0.52	313	54.8 ± 0.8	0.063 ± 7 × 10^{-4}	24.9 ± 0.2	0.998
CH_4	0.99	313	53.1 ± 0.8	0.063 ± 7 × 10^{-4}	24.9 ± 0.2	0.998
CH_4	1.50	313	56.6 ± 0.8	0.063 ± 7 × 10^{-4}	24.9 ± 0.2	0.998
CH_4	1.98	313	56.1 ± 0.8	0.063 ± 7 × 10^{-4}	24.9 ± 0.2	0.998
CH_4	0.51	338	28.4 ± 0.4	0.125 ± 2 × 10^{-3}	24.9 ± 0.2	0.998
CH_4	1.00	338	26.5 ± 0.4	0.125 ± 2 × 10^{-3}	24.9 ± 0.2	0.998
CH_4	1.51	338	27.2 ± 0.4	0.125 ± 2 × 10^{-3}	24.9 ± 0.2	0.998
CH_4	1.99	338	27.8 ± 0.4	0.125 ± 2 × 10^{-3}	24.9 ± 0.2	0.998

[a] Standard error, calculated with Origin 5.0 program

[b] 95 % confidence interval, calculated with the method proposed by Froment and Bischoff (1990)

diffusion increases and D_c/r_c^2 decreases strongly when Na^+ is replaced by Ca^{2+}, which can be attributed to the higher charge density and higher polarizability of Ca^{2+} with respect to Na^+ (Yang 2003). The effect is much stronger for carbon monoxide (K and D_c/r_c^2 change by a factor larger than 10) due to its dipole and quadrupole moments.

3.2 Measurement of adsorption equilibrium isotherms in CaX

The measured adsorption isotherms of hydrogen, nitrogen, methane and carbon monoxide on CaX pellets at 298, 313 and 338 K are presented in Fig. 2. The reversibility of all the measured isotherms is confirmed as the adsorption and desorption data fall on the same line. The experimental isotherms can be adequately reproduced by the Dual Langmuir (DL) model (Eq. (2)), as it is shown in Fig. 2.

$$n = \frac{n_{max1} b_1 p}{1 + b_1 p} + \frac{n_{max2} b_2 p}{1 + b_2 p} \quad b_1 = b_{01} \exp\left(-\frac{\Delta H_1}{RT}\right) \quad b_2 = b_{02} \exp\left(-\frac{\Delta H_2}{RT}\right) \tag{2}$$

This model was selected because it has good flexibility for fitting experimental isotherms, and it allows predicting the

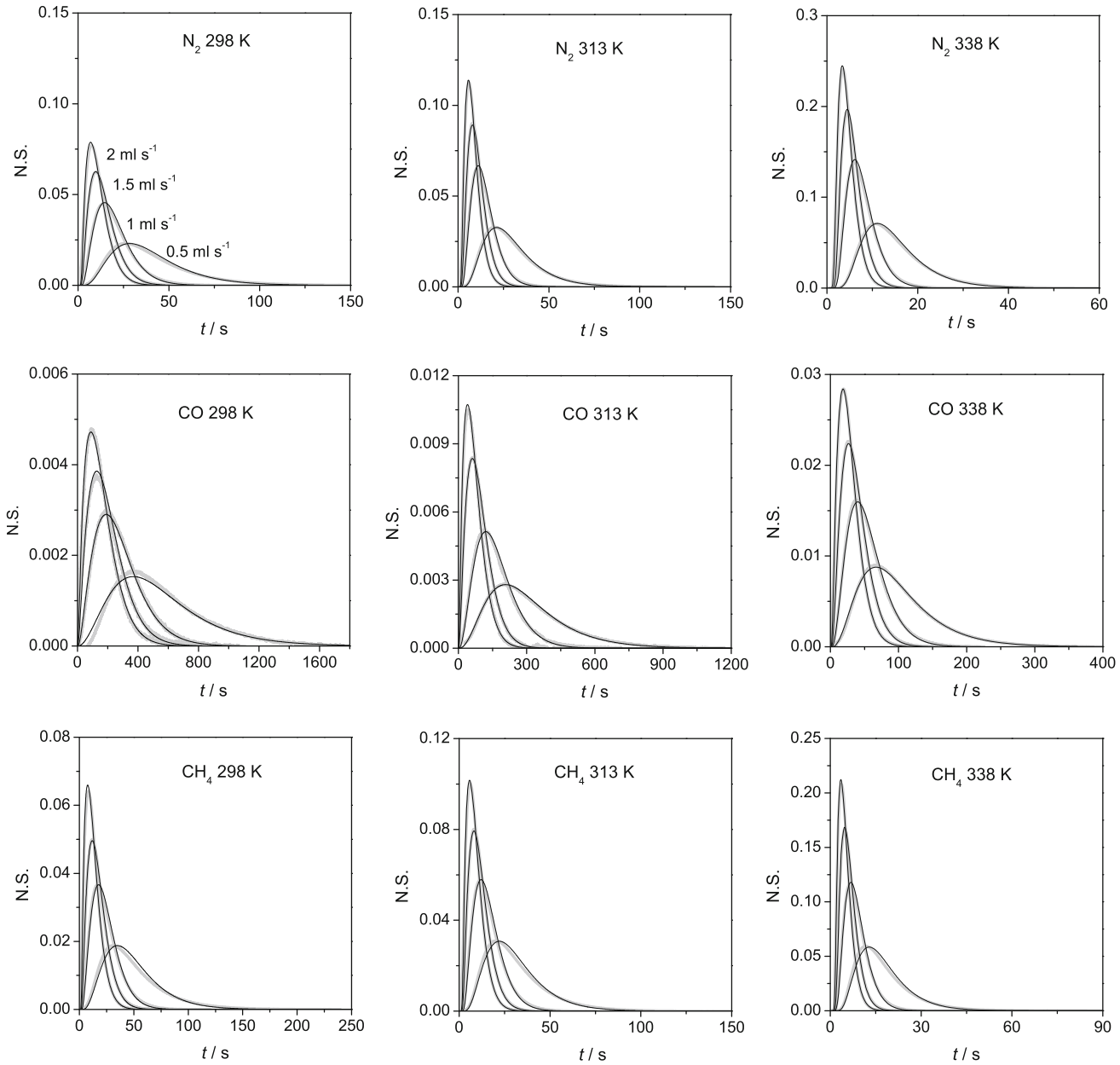

Fig. 1 Pulse responses from an bed packed with CaX pellets. *Grey lines* are the experimental signal and black lines are the theoretical signal from the model. Experimental conditions are given in Table 3. In each graph, carrier gas flow rate changes as indicated in the graph for N_2 at 298 K

Table 4 Comparison of adsorption and diffusion parameters of methane and carbon monoxide in NaX and CaX zeolites

Gas	Zeolite	$D_c/r_{c298\ K}^2$ (s^{-1})	$K_{298\ K}$	E_{diff} (kJ mol^{-1})
CH_4	NaX	0.22	33	13.8
CH_4	CaX	0.038	85	24.9
CO	NaX	0.099	72	17.1
CO	CaX	0.0029	1,095	41.4

multicomponent adsorption isotherm of gas mixtures easily using the IAS theory (Do 1998), which is used in PSA simulations. The DL parameters obtained by non-linear regression are presented in Table 5. The isosteric heats of each gas are also needed as input in the PSA simulator, calculated as average isosteric heats with Eq. (3):

$$Q_{st} = \frac{1}{n_F}\int_0^{n_F}\left(-R\frac{\partial \ln p}{\partial(1/T)}\bigg|_n\right)dn \tag{3}$$

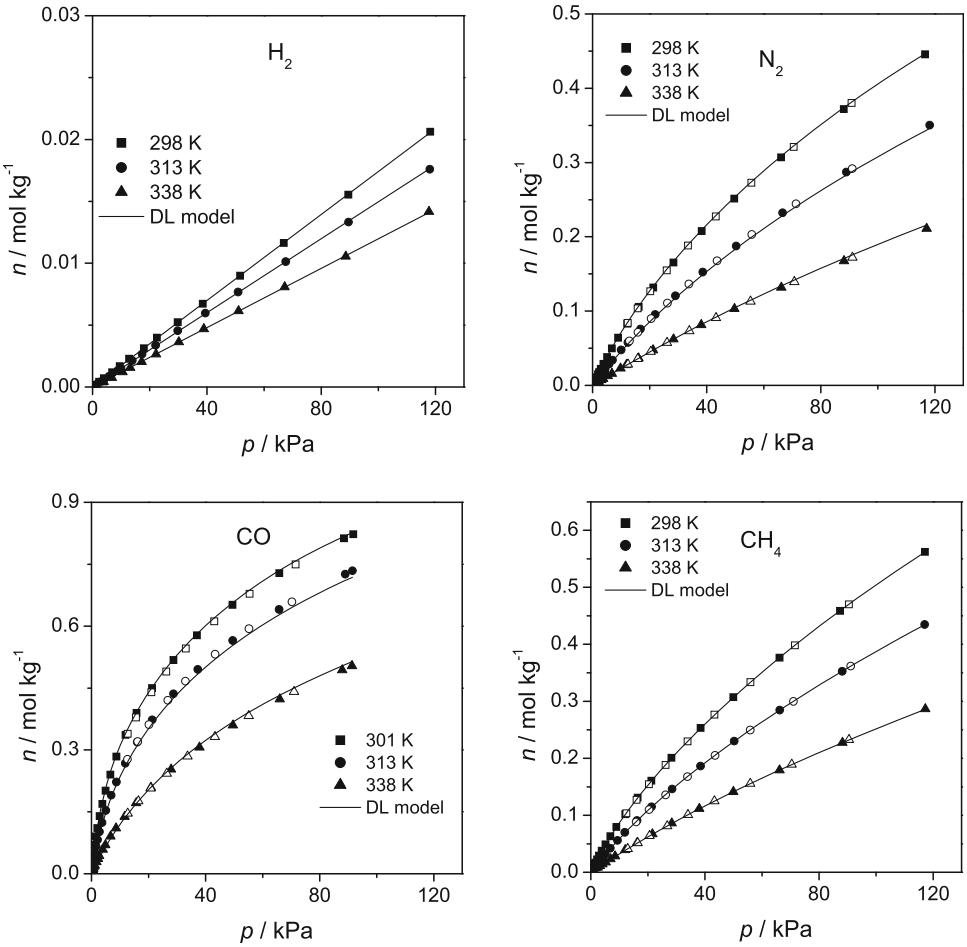

Fig. 2 Experimental adsorption isotherms of hydrogen, nitrogen, carbon monoxide and methane on CaX pellets at different temperatures. *Open symbols* depict experimental desorption equilibrium data

Table 5 Dual Langmuir parameters of the studied gases in CaX pellets

Gas	n_{max1} (mol kg^{-1})	n_{max2} (mol kg^{-1})	b_{01} (Pa^{-1})	b_{02} (Pa^{-1})	$(-\Delta H_1)$ (kJ mol^{-1})	$(-\Delta H_2)$ (kJ mol^{-1})
H_2	2.9305	0	2.4850×10^{-9}	0	7.874	0
N_2	0.08745	1.25168	5.5621×10^{-12}	1.1278×10^{-9}	39.506	20.003
CO	1.04543	0.30708	7.7365×10^{-10}	3.0671×10^{-11}	24.026	39.151
CH_4	0.10444	2.09875	1.8610×10^{-10}	1.4192×10^{-9}	31.100	18.484

where the integrand is deduced from the Dual Langmuir isotherm of each component, and n_F is the adsorption capacity calculated at feed conditions. Although the isosteric heat of adsorption depends on adsorbate loading, constant values of isosteric heat are usually assumed for simulating PSA processes (Ruthven et al. 1994). The values used for THRG and COG are given in Table 6. It is observed that the isosteric heats of nitrogen and methane are similar, whereas the value of carbon monoxide is significantly higher, which correlates with their adsorption affinities presented in Table 3.

3.3 Comparison of the adsorption isotherms of nitrogen, carbon monoxide and methane in different adsorbents

In equilibrium-based PSA separations, as the hydrogen recovery from off-gases, the adsorption isotherms of one gas in different adsorbents serve to make a preliminary comparison of their working capacity in a PSA cycle (the effective adsorbent capacity used in the cycle) for removing such gas (Lopes et al. 2010). A high adsorption capacity at feed conditions for one component contributes

Table 6 Average isosteric heats in CaX at feed conditions (3 bar, 293 K) for THRG and COG

Gas	% in THRG	% in COG	Q_{st} for THRG (kJ mol^{-1})	Q_{st} for COG (kJ mol^{-1})
H_2	69.2	57.3	7.87	7.87
N_2	26.8	10.4	23.7	25.6
CO	2.2	6.25	34.4	32.1
CH_4	1.8	26.0	24.3	20.9

positively to working capacity. However, a high curvature of the isotherm (which derives from a high adsorption affinity) contributes negatively to the working capacity because lower pressures are needed in the regeneration step (Kikkinides et al. 1993; Yang 1997; Ruthven 1984).

Higher isotherm curvature has a positive compressing effect on the mass transfer zone of the adsorption steps, because it favors a "self-sharpening" behavior in the concentration front of the adsorbate propagating along the column (Ruthven et al. 1994; Yang 1997). On the contrary, higher isotherm curvature has a negative dispersing effect on the mass transfer zone of the desorption steps, because it promotes the "proportionate pattern" behavior "in" the concentration profile, where the mass transfer zone length increases as it propagates along the column (Ruthven et al. 1994). These combined effects can be studied using PSA simulations.

Figure 3 shows the adsorption isotherms of nitrogen, carbon monoxide and methane in different zeolites (5A, CaX, 4A, NaX) and activated carbon (AC) at 293 K. The isotherms in CaX have been obtained in this work. The other isotherms have been taken from literature (5A zeolite: Tomita et al. (1987); 4A zeolite: Harper et al. (1969), multiplied by a factor of 0.8 to account for the diluting effect of binder in the other zeolites; NaX zeolite: Delgado et al. (2014) except for nitrogen, measured in this work; AC: Delgado et al. (2014) except for nitrogen, taken from Kikkinides et al. (1993). Considering the adsorption capacity in each adsorbent at equilibrium, it is expected that CaX has higher working capacity than the other ones for removing carbon monoxide when its partial pressure in the feed gas is below about 50 kPa. However, it is necessary to use PSA simulations to check this hypothesis, because it has also higher isotherm curvature, which makes the adsorbent regeneration more difficult and increases the mass transfer zone length in the desorption step, as it was discussed before.

The higher affinity of CaX towards carbon monoxide results in a higher isotherm curvature, because the saturation of the adsorption sites occurs at lower adsorptive pressures as the affinity increases. A higher adsorption affinity is indicative of a stronger adsorbent-adsorbate interaction, which is reflected on the higher heat of adsorption of carbon monoxide on CaX (34 kJ mol^{-1}, estimated from an Arrhenius plot of K values in Table 3)

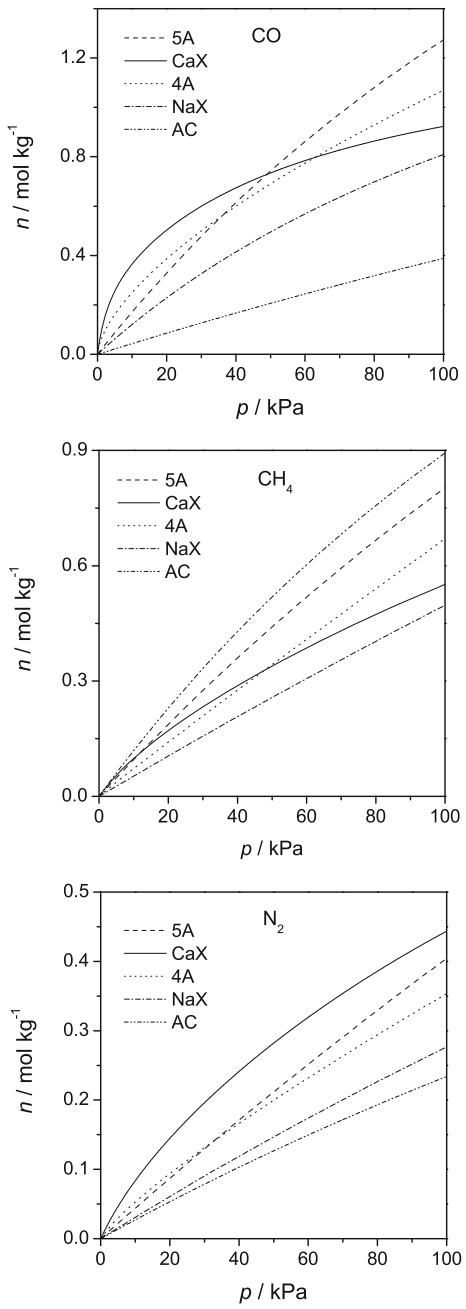

Fig. 3 Comparison of the adsorption isotherms of carbon monoxide, methane and nitrogen in different zeolites and activated carbon at 293 K

with respect to other adsorbents (33 kJ mol^{-1} in 4A Harper et al. 1969, 29 kJ mol^{-1} in 5A, 17 kJ mol^{-1} in AC Park et al. 2000, 23 kJ mol^{-1} in NaX Delgado et al. 2014).

4A zeolite has a carbon monoxide adsorption capacity higher than 5A zeolite for partial pressures below 30 kPa, but also higher isotherm curvature, which is consistent with the higher adsorption heat in 4A commented previously. NaX and AC have significantly lower carbon monoxide adsorption capacity.

In the case of methane, it is expected that AC has the highest working capacity in all the studied pressure range. This can be ascribed to the non-polar character of activated carbon surface. Among zeolites, 5A has clearly the highest working capacity for feed partial pressures above 12 kPa. Below this limit, CaX has an adsorption capacity similar to that of 5A, but a worse performance of CaX is expected because its isotherm curvature is higher. 4A zeolite can also perform better than CaX for partial pressures above 45 kPa. NaX zeolite has lower methane adsorption capacity than 4A zeolite, suggesting that the polarizing effect of sodium on methane is lower in NaX zeolite.

In the case of nitrogen, CaX has higher adsorption capacity than the rest of adsorbents in all the studied pressure range, but it has also higher isotherm curvature. 5A and 4A zeolites have a similar nitrogen adsorption capacities, higher than the ones of NaX and AC.

Among these impurities, carbon monoxide is the one with the highest affinity, so it has the strongest effect on the adsorption capacities of the other impurities. On this basis, the feed gas pressure employed in the comparison with PSA simulations was selected by analyzing the carbon monoxide isotherms. A feed pressure of 3 bar was chosen, because it results in feed carbon monoxide partial pressures where CaX has the higher adsorption capacity among the studied adsorbents (CO partial pressures = 6.6 kPa and 19 kPa for THRG and COG, respectively).

3.4 Validation of PSASIM model with experimental PSA data

The program employed for comparing the PSA performances of CaX and 5A zeolites, called PSASIM, has been validated with experimental PSA results of the recovery of hydrogen from THRG using 5A zeolite reported by Tomita et al. (1987). This program is a propietary simulator developed by Universidad Complutense de Madrid, and commercialized by Inprocess Technology and Consulting (Spain).

The model implemented in this program is derived from mass, energy and momentum balances performed in a differential portion of the adsorbent column. Model equations are presented in Table 7. The partial differential equations are discretized using the orthogonal collocation in finite ellements method, with third order Hermite polynomials, and the resulting ordinary differential equations system is solved a public domain ODE solver (ODEPACK, Hindmarsh 2006). Danckwert's boundary conditions are imposed in each step of the PSA cycle, and linear pressure variations are assumed in pressure-changing steps. The reported PSA cycle operates with four columns, where each column undergoes the sequence of steps indicated in Fig. 4. The meaning of the abbreviations is the following:

ADS	Adsorption step. Feed gas is introduced at high pressure, and light product is obtained
DEQ 1	Depressurizing equalization 1. Column is depressurized in parallel, and the released gas is used to pressurize other column
PP	Provide purge. Column is depressurized in parallel, and the released gas is used to purge other column
DEQ 2	Depressurizing equalization 2. As DEQ 1, starting from the final pressure of PP step
BD	Blowdown. Column is depressurized down to the low pressure in the cycle countercurrently, and tail gas is released
RP	Receive purge. Column is purged countercurrently with the gas released from PP step. More tail gas is released
PEQ 2	Pressurizing equalization 2. Column is pressurized countercurrently with the gas released from DEQ 2 step
PEQ 1	Pressurizing equalization 1. Column is pressurized countercurrently with the gas released from DEQ 1 step
BF	Backfill. Column is pressurized countercurrently up to high pressure with a portion of light product gas

The composition of feed gas is shown in Table 6. Experimental final step pressures are given in Fig. 4b, which were introduced in the simulator. The final pressures of PEQ 1 and PEQ 2 steps are calculated by the model, depending on the amounts of gas released from DEQ 1 and DEQ 2 steps. Bed and adsorbent properties are shown in Table 8. Experimental purity and recovery results in different experiments are presented in Table 9. These parameters were calculated in the model as follows (at the cyclic steady state):

$$\text{Purity} = \frac{(\text{moles } H_2 \text{ out})_{ADS} - (\text{moles } H_2 \text{ in})_{BF}}{(\text{moles out})_{ADS} - (\text{moles in})_{BF}} \times 100 \quad (4)$$

$$\text{Recovery} = \frac{(\text{moles } H_2 \text{ out})_{ADS} - (\text{moles } H_2 \text{ in})_{BF}}{(\text{moles } H_2 \text{ in})_{ADS}} \times 100 \quad (5)$$

The composition of the gas used in the backfill step and that of the light product (the product in ADS step) are the same because a portion of light product is used in

Table 7 Model for a PSA process

Total mass balance in voids between particles

$$\varepsilon \frac{\partial C}{\partial t} = -\frac{\partial}{\partial z}(uC) - (1-\varepsilon)\frac{3}{R_p}\sum_{i=1}^{i=n} k_{macro,i}\left(Cy_i - c_{macro,i}\right)$$

Mass balance of ith component in voids between particles

$$\varepsilon \frac{\partial (Cy_i)}{\partial t} = -\frac{\partial}{\partial z}(u\,Cy_i) + D_L\varepsilon\frac{\partial}{\partial z}\left(C\frac{\partial y_i}{\partial z}\right) - (1-\varepsilon)\frac{3}{R_p}k_{macro,i}\left(Cy_i - c_{macro,i}\right)$$

Mass balance in macropores

$$\varepsilon_p \frac{\partial c_{macro,i}}{\partial t} = \frac{3}{R_p}k_{macro,i}\left(Cy_i - c_{macro,i}\right) - \rho_p 15\left(\frac{D_e}{r_c^2}\right)_i\left(n_i^* - n_i\right)$$

Mass balance in micropores

$$\frac{\partial n_i}{\partial t} = 15\left(\frac{D_e}{r_c^2}\right)_i\left(n_i^* - n_i\right)$$

Equation of state

$$C = \frac{P}{RT_g}$$

Momentum balance

$$-\frac{\partial P}{\partial z} = \frac{150\mu(1-\varepsilon)^2}{\varepsilon^3 4R_p^2}u + \frac{1.75\,(1-\varepsilon)\rho_g}{\varepsilon^3 2R_p}u^2$$

Energy balance in voids between particles

$$\frac{\partial}{\partial t}\left(\varepsilon c_{vg}CT_g\right) = \lambda\frac{\partial^2 T}{\partial z^2} - \frac{\partial}{\partial z}\left(u\,C\,c_{pg}T_g\right) + (1-\varepsilon)\frac{3}{R_p}h_{sg}\left(T_s - T_g\right) - \frac{2}{R_w}h_w\left(T_g - T_w\right)$$

Energy balance in adsorbent particles

$$\frac{\partial}{\partial t}\left(\rho_p c_{ps}T_s + \varepsilon_p c_{vg}T_s\sum_{i=1}^{i=n} c_{macro,i}\right) = \rho_p\sum_{i=1}^{i=n}\left(Q_{st,i}\frac{\partial n_i}{\partial t}\right) - \frac{3}{R_p}h_{sg}\left(T_s - T_g\right)$$

Energy balance in column wall

$$\frac{\partial}{\partial t}\left(\rho_w c_{pw}T_w\right) = \frac{2\pi R_w}{S_w}h_w\left(T_g - T_w\right) - \frac{2\pi(R_w+e_w)}{S_w}U(T_w - T_{ext})$$

Multicomponent adsorption isotherm (IAST)

$$Py_i = p_i^o(\pi)x_i \quad \pi = \pi_1 = \cdots = \pi_n \quad \pi_i = \int_0^{p_i^o}\frac{n_i^o}{p_i^o}dp_i^o \quad \frac{1}{n_T} = \sum_1^n\frac{x_i}{n_i^o\left(p_i^o\right)} \quad n_i = n_T x_i$$

Gas–solid heat transfer correlation

$$h_{sg} = \frac{k_g}{2R_p}\left(2 + 1.1\,Re^{0.6}Pr^{1/3}\right)$$

Gas–solid mass transfer correlation

$$k_f = \frac{u}{\varepsilon Sc^{2/3}}\left(\frac{0.765}{Re^{0.82}} + \frac{0.365}{Re^{0.386}}\right)$$

Gas-macropore mass transfer coefficient

$$k_{macro} = \left(\frac{1}{\frac{5D_m\varepsilon_p}{\tau R_p}} + \frac{1}{k_f}\right)^{-1}$$

Axial dispersion correlation

$$D_L = 0.73\,D_m + \frac{u R_p/\varepsilon}{1+\frac{9.49\varepsilon D_m}{2uR_p}}$$

the backfill step (Fig. 4a). Model parameters introduced in the program to simulate the PSA experiments are presented in Table 10. The Langmuir parameters for nitrogen, carbon monoxide and methane have been taken from Tomita et al. (1987), and the ones of hydrogen from Park et al. (2000). It was assumed that Langmuir parameters in the studied conditions do not depend on temperature, as it was assumed by Tomita et al. (1987) in the model employed in their work (Continuous Countercurrent Flow Model, CCFM). It was also assumed that gas-adsorbent mass transfer is controlled by macropore diffusion.

From the comparison of experimental and simulated results in Table 9, it is observed that PSASIM program predicts with reasonable accuracy the experimental purity and recovery results, for a wide range of operating conditions. As the model is based in conservation and fundamental equations, it can be used for screening other adsorbents and making a preliminary design of other PSA cycles.

3.5 Comparison of the performance of CaX and 5A zeolites in the recovery of hydrogen from THRG and COG

The performances of CaX and 5A zeolites in a PSA cycle for recovering hydrogen from THRG and COG have been simulated with PSASIM. The same four-column PSA cycle as the one studied by Tomita et al. (1987) has been considered (Fig. 4), working between 1 and 3 bar. Cycle time schedule, bed length, and bed radius are the same as in Run 1 in Table 9 ($t_1 = 45$ s, $t_2 = 105$ s, $t_3 = 30$ s in Fig. 4b, bed length = 2 m, bed radius = 2.15 cm). Feed and surroundings temperature are 293 K. The different particle densities (1,182 and 1,360 kg m^{-3} for 5A and CaX zeolites, respectively) and particle porosities (0.55 and 0.47, respectively) of both adsorbents are used in the model, but the same particle size is assumed for both adsorbents to remove the effect of this variable (1.5 mm). Macropore diffusion is calculated with a molecular diffusivity of 2.25×10^{-5} m^2 s^{-1} in both adsorbents. Equilibrium parameters and reciprocal diffusion

(a)

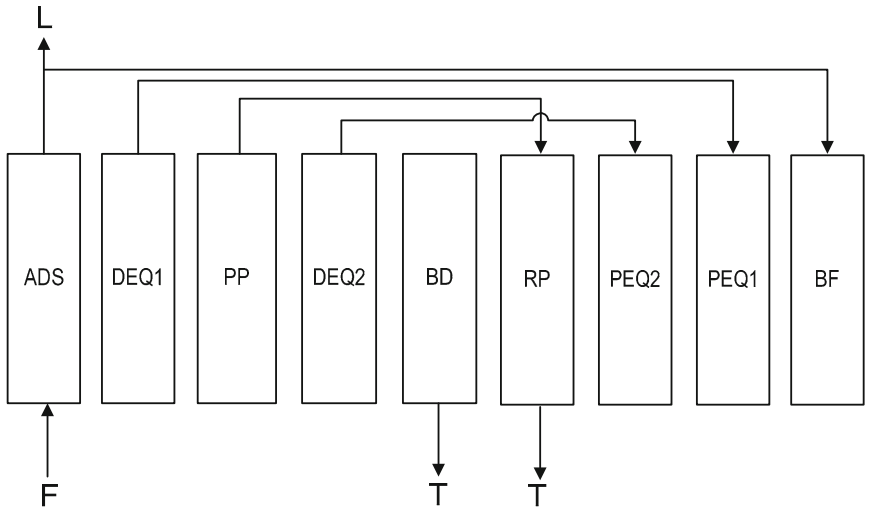

(b)

Duration	t_1	t_2	t_3	t_1	t_2	t_3	t_1	t_2	t_3	t_1	t_2	t_3
Step	1			2	3	4	5	6	7	8	9	
Final press., bar	8.4			5.1	2.3	1.9	1.5	1.5	1.9	5.0	8.4	
COLUMN 1	ADS			DEQ1	PP	DEQ2	BD	RP	PEQ2	PEQ1	BF	
COLUMN 2	PEQ1	BF		ADS			DEQ1	PP	DEQ2	BD	RP	PEQ2
COLUMN 3	BD	RP	PEQ2	PEQ1	BF		ADS			DEQ1	PP	DEQ2
COLUMN 4	DEQ1	PP	DEQ2	BD	RP	PEQ2	PEQ1	BF		ADS		

Fig. 4 PSA cycle studied by Tomita et al. (1987). **a** Connectivity between steps. F = feed gas, L = light product (hydrogen-rich), T = tail gas (rich in impurities). **b** Cycle time schedule. The ratios between t_1, t_2 and t_3 were constant in all the experiments ($t_1 = 1.5\ t_3$, $t_2 = 3.5\ t_3$). The cycle duration is 4 ($t_1 + t_2 + t_3$). The final pressure is the pressure reached at the end of each step in COLUMN 1 for Run 1 in Table 9

Table 8 Bed and adsorbent properties in the PSA experiments reported by Tomita et al. (1987)

Adsorbent	5A Zeolite (Baylith K-154)
Shape	Spherical beads
Average particle radius	1.35 mm
Total bed porosity	0.73
Bed density	688.6 kg m^{-3} (1 m column), 709.3 kg m^{-3} (2 m column)
Bed porosity between particles	0.4
Bed radius	2.15 cm

constants in Tables 3, 5 and 6 are introduced in the program for CaX zeolite. The equilibrium and diffusion parameters in Table 10 are used for 5A zeolite. The effect of loading on the micropore diffusion coefficients has been neglected for the sake of simplicity (Ruthven et al. 1994). This assumption has been considered previously in the literature for simulating PSA processes (Da Silva and Rodrigues 2001; Jayaraman et al. 2004).

The PSA cycles have been designed considering as design specifications that the carbon monoxide concentration in the hydrogen product must be below 100 ppm (Yang et al. 1997; Chou et al. 2013), and that the hydrogen purity must be higher than 99.7 % (as in Run 1 in Table 9). The manipulated variable was the superficial velocity in the adsorption (ADS) step (u_F = volumetric flow rate/column section). The final pressure of the provide purge (PP) step was set to 1.6 bar in all the simulations because it was observed that changing this parameter around this value had a weak effect on the performance results (after manipulating u_F to reach a purity close to 99.7 %).

The final pressures in DEQ 1, DEQ 2, PEQ 1 and PEQ 2 are calculated by the program imposing the conditions that the final pressure in each DEQ step is equal to the one of the corresponding PEQ step, and that the mole flow rate histories of each component in the gas released from each DEQ step are equal to mole flow rate histories

Table 9 Comparison between PSA experimental results reported by Tomita et al. (1987), and results simulated with PSASIM program, introducing the experimental operation conditions as input the program

Run	u_F (m s^{-1})[a]	L (m)	Cycle duration (min)	H_2 purity exp (%)	H_2 purity sim (%)	Recovery exp (%)	Recovery sim (%)
1	0.0224	2	12	99.73	99.79	77.7	78.04
2	0.0219	2	24	85.61	91.04	88.4	91.06
3	0.0219	2	48	76.19	78.33	94.9	95.75
4	0.0316	2	8.4	99.38	99.58	77.2	77.8
5	0.0314	2	33.6	76.55	78.25	94.6	95.73
6	0.0125	2	21	99.93	99.95	77.7	77.14
7	0.0219	1	4.7	99.87	99.66	70.0	69.77
8	0.0219	1	6	97.93	98.92	78.6	78.02

[a] Feed superficial velocity in ADS step

Table 10 Model parameters introduced in PSASIM program for simulating PSA results with 5A zeolite reported by Tomita et al. (1987)

Gas viscosity	1.3×10^{-5} Pa s
Gas heat conductivity	0.1 W m^{-1} K^{-1}
Gas heat capacity at constant pressure	32 J mol^{-1} K^{-1}
Gas heat capacity at constant volume	23 J mol^{-1} K^{-1}
Adsorbent heat capacity	1,000 J kg^{-1} K^{-1}
Molecular diffusivity	8×10^{-6} m^2 s^{-1}
Particle porosity	0.55
Tortuosity	3
Maximum Peclet number for axial dispersion	500
Feed and surroundings temperature	293 K
Isosteric heats of adsorption	
H_2	6.22 kJ mol^{-1}
N_2	18.9 kJ mol^{-1}
CO	29.1 kJ mol^{-1}
CH_4	19.4 kJ mol^{-1}
Langmuir parameters at 293 K	
$n_{maxH2} = 2.47$ mol kg^{-1}	$b_{H2} = 8.63 \times 10^{-8}$ Pa^{-1}
$n_{maxN2} = 4.5$ mol kg^{-1}	$b_{N2} = 9.87 \times 10^{-7}$ Pa^{-1}
$n_{maxCO} = 4.5$ mol kg^{-1}	$b_{CO} = 3.95 \times 10^{-6}$ Pa^{-1}
$n_{maxCH4} = 4.5$ mol kg^{-1}	$b_{CH4} = 2.17 \times 10^{-6}$ Pa^{-1}
$(D_c/r_c)^2$ = infinite for all components	
Column wall thickness	2 mm
Column wall heat capacity	500 J kg^{-1} K^{-1}
Column wall density	8,000 kg m^{-3}
Wall-gas heat transfer coefficient	60 W m^{-2} K^{-1}
Wall-surroundings heat transfer coefficient	2 W m^{-2} K^{-1}

entering the column in the corresponding PEQ step. The same occurs with the mole flow rate histories in the PP and RP steps.

The performance parameters considered in the comparison are the hydrogen purity and recovery, calculated with Eqs. (4) and (5), and productivity, calculated with Eq. (6):

$$\text{Productivity} = \frac{(\text{moles } H_2 \text{ out})_{\text{ADS}} - (\text{moles } H_2 \text{ in})_{\text{BF}}}{(\text{cycle time})(\text{mass of adsorbent in one column})} \quad (6)$$

Simulation results are presented in Table 11. The performance of CaX and 5A zeolites in the hydrogen recovery from THRG with the PSA cycle in Fig. 4 is compared in

Table 11 Design parameters and simulated PSA performance results

Simulation	Cycle	Ads.	Gas	u_F (m s^{-1})	t_{RIN} (s)	Pur. (%)	CO (ppm)	N_2 (ppm)	CH_4 (ppm)	Rec. (%)	Productivity, (mol_{H2} kg^{-1} s^{-1})
1	Figure 4	CaX	THRG	0.0110	–	99.75	21	2,425	45	65.4	9.30×10^{-5}
2	Figure 4	5A	THRG	0.0120	–	99.75	0	2,464	0	65.2	1.16×10^{-4}
3	Figure 4	CaX	COG	0.0120	–	99.87	35	878	374	66.2	8.60×10^{-5}
4	Figure 4	5A	COG	0.0130	–	99.85	0	1,527	5	62.4	1.01×10^{-4}
5	Figure 6	CaX	THRG	0.0140[a]	100	99.71	31	2,845	13	93.4	7.61×10^{-5}
6	Figure 6	5A	THRG	0.0154[a]	100	99.71	0	2,856	0	90.5	9.30×10^{-5}
7	Figure 6	CaX	COG	0.0150[a]	100	99.79	69	1,837	153	92.0	6.65×10^{-5}
8	Figure 6	5A	COG	0.0190[a]	100	99.75	0	2,526	4	88.4	9.29×10^{-5}

[a] The same value for ADS and RIN steps

Simulations 1 and 2. The performance in the hydrogen recovery from COG is compared in Simulations 3 and 4.

It is observed that CaX zeolite results in higher recovery than 5A zeolite for the same (or higher) hydrogen purity. CaX removes nitrogen better than 5A zeolite, particularly from COG, but it performs worse with carbon monoxide and methane. The productivity is slightly higher with 5A zeolite, which is due in part to its lower density, so a lower mass of adsorbent is employed in Eq. (6). The higher working capacities of 5A zeolite for carbon monoxide and methane also contribute to its higher productivity. Figure 5a shows the spatial profiles of gas mole fractions at the end of ADS step with THRG as feed for both zeolites. This graph shows the gas composition inside the bed at end of the production of light product. Figure 5b shows the spatial profiles of adsorbed concentration with THRG at the end of RP step. This graph shows the bed content at the end of the regeneration process. Figure 5c, d show the equivalent graphs for COG as feed.

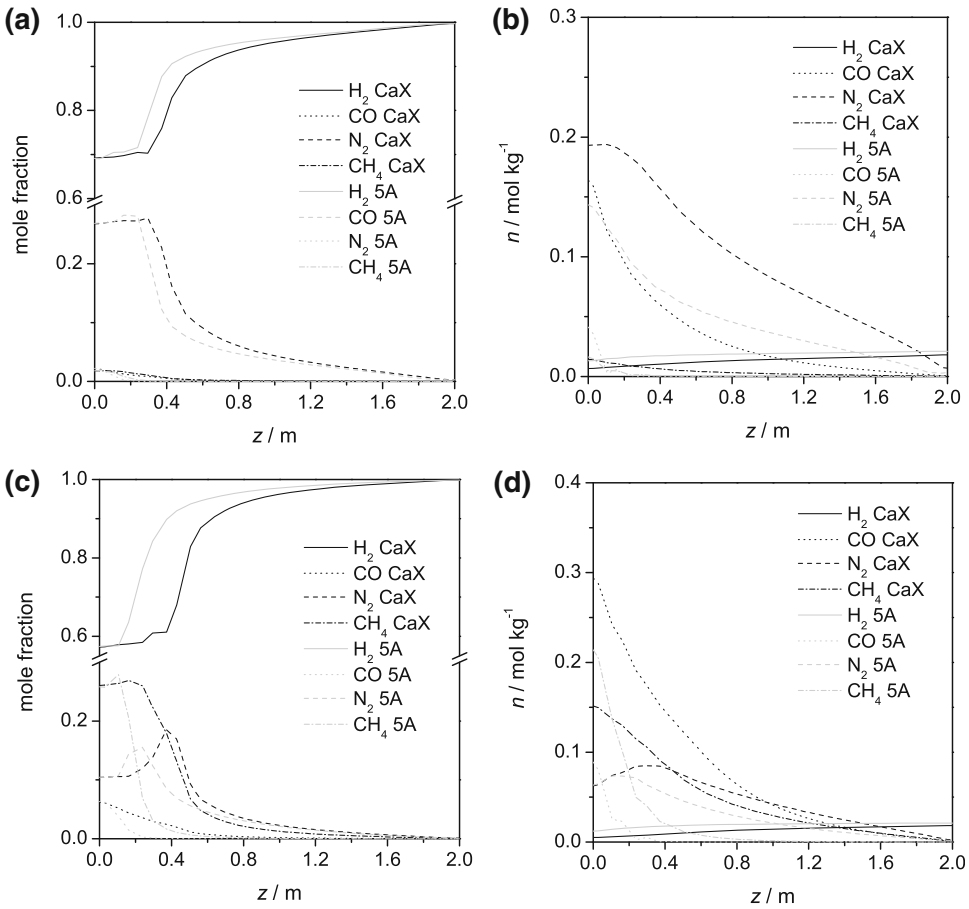

Fig. 5 Simulated spatial profiles of gas mole fractions and adsorbed concentrations for the PSA cycle in Fig. 4. **a** Gas mole fractions at the end of the ADS step with THRG as feed. **b** Adsorbed concentrations at the end of the RP step with THRG as feed. **c** Gas mole fractions at the end of the ADS step with COG as feed. **d** Adsorbed concentrations at the end of the RP step with COG as feed

(a)

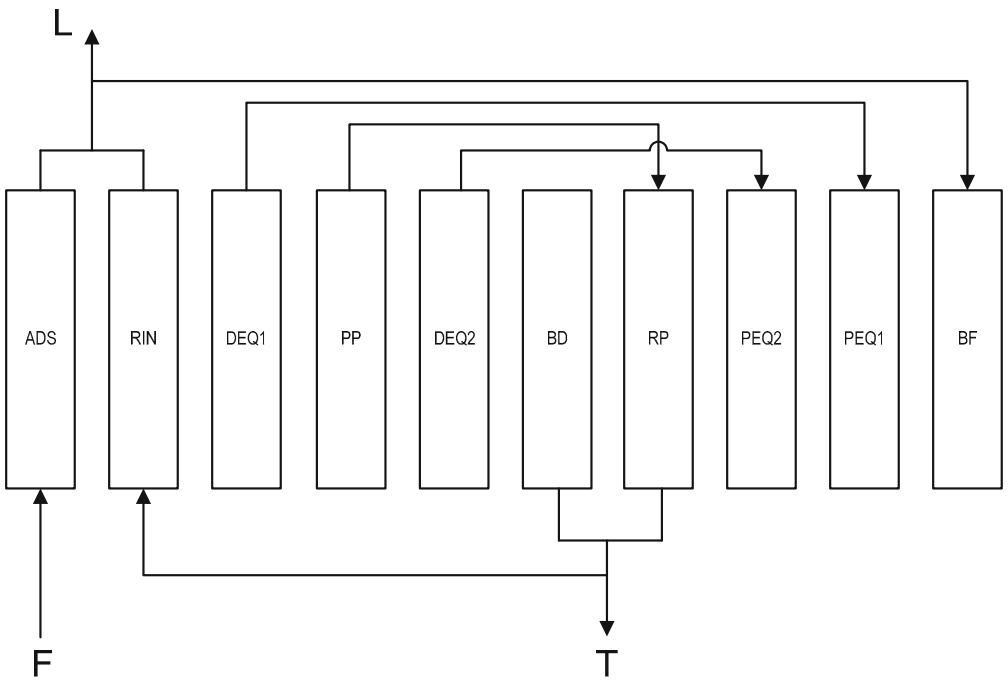

(b)

Duration, s	80	100	45	105	30	45	105	30	45	135
Step	1	2	3	4	5	6	7	8	9	10
Final press., bar	3.0	3.0	2.1	1.6	1.3	1.0	1.0	1.3	2.1	3.0
COLUMN 1	ADS	RIN	DEQ1	PP	DEQ2	BD	RP	PEQ2	PEQ1	BF
COLUMN 2	PEQ1	BF	ADS	RIN		DEQ1	PP	DEQ2	BD	RP PEQ2
COLUMN 3	BD	RP PEQ2	PEQ1	BF		ADS	RIN		DEQ1	PP DEQ2
COLUMN 4	DEQ1	PP DEQ2	BD	RP	PEQ2	PEQ1	BF		ADS	RIN

Fig. 6 PSA cycle resulting from introducing a rinse (RIN) step in the PSA cycle presented in Fig. 4. **a** Connectivity between steps. F = feed gas, L = light product, T = tail gas. **b** Cycle time schedule. The final pressure is the pressure reached at the end of each step in COLUMN 1 for Simulation 5 in Table 11

From Fig. 5a, c, it is inferred that the higher hydrogen recovery obtained with CaX occurs because the concentration waves of impurities propagate a longer distance during the ADS step with this adsorbent. As a result, the loading of impurities in the column at the start of the regeneration process is higher, and the hydrogen concentration in the tail gas is lower, which eventually results in a higher hydrogen recovery.

The longer propagation distance of impurities can be attributed to the higher curvatures of the isotherms on CaX (Fig. 3), deriving from a higher sorption affinity. A high isotherm curvature results in the accumulation of impurities in the column when the PSA cycle reaches the cyclic steady state, because their desorption is more difficult. As the column starts the ADS step with a higher loading of impurities, the available adsorption capacity is lower, resulting in a longer propagation distance at the end of this step. Two examples of accumulation of impurities can be observed in the PSA processes studied by Park et al. (2000) and Delgado et al. (2014), where carbon dioxide accumulates on 5A zeolite and NaX zeolite, respectively. The carbon dioxide isotherms in these adsorbents are highly curved.

In spite of the higher loading of impurities in CaX at end of ADS step, the same hydrogen purity is obtained with 5A and CaX zeolites (Simulations 1 and 2 in Table 11). This is again due to the higher curvatures of the isotherms of the impurities in CaX (Fig. 3), which result in shorter mass transfer zones in the concentration profiles during adsorption. The reducing effect of the isotherm curvature on the mass transfer zone length in an adsorption column can be deduced using a theoretical model based on the constant-pattern assumption (Wankat 1994; Sircar and Kumar 1983), where the isotherm curvature is quantified with the adsorption affinity parameter in the Langmuir isotherm equation.

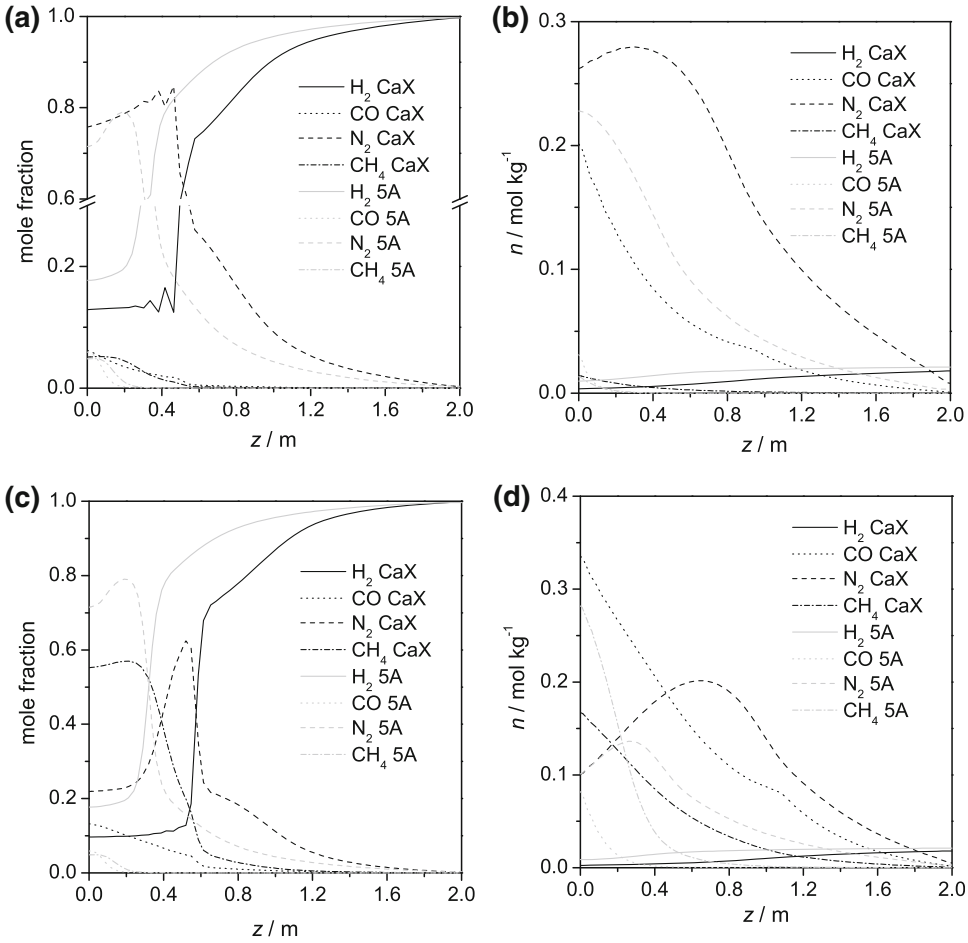

Fig. 7 Simulated spatial profiles of gas mole fractions and adsorbed concentrations for the PSA cycle in Fig. 6. **a** Gas mole fractions at the end of the RIN step with THRG as feed. **b** Adsorbed concentrations at the end of the RP step with THRG as feed. **c** Gas mole fractions at the end of the RIN step with COG as feed. **d** Adsorbed concentrations at the end of the RP step with COG as feed

From Fig. 5b, d, it is deduced that the accumulation of impurities in the second half of the column (near the light product end) in 5A zeolite is lower than in CaX zeolite, particularly for carbon monoxide and methane. This explains higher working capacities obtained with 5A zeolite for carbon monoxide and methane. Their desorption is easier, which comes from the lower curvatures of their isotherms.

Although the studied PSA cycle can produce hydrogen with the required purity specifications with both zeolites, the hydrogen recovery is quite low (below 70 %). One way of increasing light product recovery while maintaining high light product purity is to include a rinse step in the cycle, i.e., recycling a portion of heavy product as feed (Delgado et al. 2013). Introducing this change in the cycle makes it similar to a Dual-Reflux PSA process (Kearns and Webley 2006), where portions of both light and heavy products are recycled in the PSA process.

Figure 6 shows the connectivity between steps and the cycle time schedule of the modified PSA cycle. The difference with the PSA cycle in Fig. 4 is the inclusion of a rinse step after the adsorption step, where a portion of the tail gas is fed to the column at high pressure (3 bar). The modified PSA cycle was designed using the same operating conditions and design specifications as in Simulations 1–4 in Table 11, but leaving as manipulated variables the duration of the rinse step (keeping the sum of the durations of ADS and RIN steps equal to 180 s), and the feed superficial velocity of the ADS and RIN steps (using the same velocity in both steps).

The design results and the resulting performance parameters with CaX and 5A zeolites as adsorbents, and THRG and COG as feed, are presented in Table 11 (Simulations 5, 6, 7 and 8). The results are qualitatively the same as the ones observed previously with the original PSA cycle: (1) for a similar product purity, CaX zeolite gives a higher recovery than 5A zeolite, particularly with COG as feed (2) CaX zeolite removes nitrogen better than 5A zeolite. However, much higher recovery is obtained with the inclusion of the rinse step (around 90 %).

Figure 7a show the spatial profiles of gas mole fractions at the end of the RIN step, and Fig. 7b the ones of adsorbed concentration at the end of RP step, when the feed is THRG. Figure 7c, d show the same profiles when the feed is COG. Again, the reason for the higher recovery with CaX is due to the higher loading of impurities with this

zeolite with both kinds of feed. The gas composition at $z = 0$ in Figs. 7a, c corresponds to the gas composition of the tail gas (as deduced from Fig. 6a).

It is observed that the hydrogen concentration in the tail gas is significantly lower with CaX zeolites with both THRG and COG as feed, which results in a higher recovery. The higher recovery is obtained at the cost of a lower productivity (Table 11), although the reduction is not very strong (around 20 %). The lower productivity occurs because the inclusion of the rinse step implies that a lower amount of fresh feed enters the process in each cycle.

Figure 7b, d show that again 5A zeolite has a lower accumulation of impurities in the second half of the column, due to the lower curvature of the isotherms in this zeolite. In spite of this, CaX zeolite results in the same product purity also with the modified PSA cycle, for the reasons commented previously.

4 Conclusions

Hydrogen recovery from off-gases with nitrogen-rich impurity (THRG and COG) by PSA with CaX and 5A zeolites has been studied using a simulation tool (PSASIM).

To simulate the PSA process with CaX, the reciprocal diffusion time constants of nitrogen, methane and carbon monoxide in this adsorbent have been measured experimentally.

The adsorption isotherms of hydrogen, nitrogen, methane and carbon monoxide in CaX have also been measured experimentally for the same purpose. They can be reproduced using the Dual Langmuir model.

From a comparison between the adsorption isotherms in CaX and other adsorbents (5A zeolite, 4A zeolite, NaX zeolite, AC), it is expected that CaX can give a better separation performance in the studied PSA process when the feed gas pressure is 3 bar.

The separation performances of CaX and 5A zeolites in the hydrogen recovery from THRG and COG by PSA have been compared for a feed gas pressure of 3 bar. According to the simulated results, CaX leads to higher hydrogen recovery than 5A zeolite for the same product purity (above 99.7 %) with both feed gases.

CaX removes nitrogen better than 5A zeolite, although it is worse for removing carbon monoxide and methane because of the different curvature of the isotherms in both adsorbents. The hydrogen recovery is increased notably by including a rinse step in the cycle, without reducing the product purity.

Although the PSA results reported here are theoretical, they show the potential benefit of using CaX zeolite for recovering hydrogen from off-gases with nitrogen-rich impurity. Hence, it is recommended to study the proposed PSA processes experimentally.

Acknowledgments Financial support from the Ministry of Economy and Competitiveness of Spain through project CTQ2012-34626 is gratefully acknowledged.

References

Ahn, H., Yang, J., Lee, C.H.: Effects of feed composition of coke oven gas on a layered bed H2 PSA process. Adsorption **7**, 339–356 (2001)

Baksh, M.S.A., Simo, M.: Ten bed pressure swing adsorption process operating in normal and turndown modes. U. S. Patent 8,435,328 (2013)

Bakta, M.: Moderate excess nitrogen Braun Purifier™ process and method for retrofitting non-Braun Purifier™ ammonia plants, U.S. Patent 5935544 (1999)

Barg, C., Ferreira, J.M.P., Trierweiler, J.O., Secchi, A.R.: Simulation and optimization of an industrial PSA unit. Braz. J. Chem. Eng. **17** (2000). doi:10.1590/S0104-66322000000400033

Beaver, M.G., Sircar, S.: Decentralized production of hydrogen for residential PEM fuel cells from piped natural gas by low temperature steam-methane reforming using sorption enhanced reaction concept. In: Eguchi, K. (ed.) Clean Energy Systems and Experiences. ISBN: 978-953-307-147-3, Intech (2010)

Besancon, B.M., Hasanov, V., Imbault-Lastapis, R., Benesch, R., Barrio, M., Mølnvik, M.J.: Hydrogen quality from decarbonized fossil fuels to fuel cells. Int. J. Hydrogen Energy **34**, 2350–2360 (2009)

Biswas, P., Agrawal, S., Sinha, S.: Modeling and simulation for pressure swing adsorption system for hydrogen purification. Chem. Biochem. Eng. Q. **24**, 409–414 (2010)

Casas, N., Schell, J., Joss, L., Mazzotti, M.: A parametric study of a PSA process for pre-combustion CO_2 capture. Sep. Purif. Technol. **104**, 183–192 (2013)

Chen, Y., Fair, G.: Processes for the recovery of high purity hydrogen and high purity carbon dioxide. US Patent 8394174 B2 (2013)

Chlendi, M., Tondeur, D.: Dynamic behavior of layered columns in pressure swing adsorption. Gas Sep. Pur. **9**, 231–242 (1995)

Chou, C.T., Chen, F.H., Huang, Y.J., Yang, H.S.: Carbon dioxide capture and hydrogen purification from synthesis gas by pressure swing adsorption. Chem. Eng. Trans. **32**, 1855–1860 (2013)

Cormos, C.C., Starr, F., Tzimas, E., Peteves, S.: Innovative concepts for hydrogen production processes based on coal gasification with CO_2 capture. Int. J. Hydrogen Energy **33**, 1286–1294 (2008)

Da Silva, F.A., Rodrigues, A.E.: Propylene/propane separation by vacuum swing adsortion using 13X zeolite. AIChE J. **47**, 341–357 (2001)

Delgado, J.A., Águeda, V.I., Uguina, M.A., Sotelo, J.L., Fernández, P.: Adsorption and diffusion of nitrogen, methane and carbon dioxide in aluminophosphate molecular sieve $AlPO_4$-11. Adsorption **19**, 407–422 (2013)

Delgado, J.A., Agueda, V.I., Uguina, M.A., Sotelo, J.L., Brea, P., Grande, C.A.: Adsorption and diffusion of H_2, CO, CH_4, and CO_2 in BPL activated carbon and 13X zeolite: evaluation of performance in pressure swing adsorption hydrogen purification by simulation. Ind. Eng. Chem. Res. (2014). doi:10.1021/ie403744u

Do, D.D.: Adsorption Analysis: Equilibria and Kinetics. Imperial College Press, Singapore (1998)

Dowling, A.W., Vetukuri, S.R.R., Biegler, L.T.: Large-scale optimization strategies for pressure swing adsorption cycle synthesis. AIChE J. **58**, 3777–3791 (2012)

Froment, G.F., Bischoff, K.B.: Chemical Reactor Analysis and Design. Wiley, New York (1990)
Harper, R.J., Stifel, G.R., Anderson, R.B.: Adsorption of gases on 4A synthetic zeolite. Can. J. Chem. **47**, 4661–4670 (1969)
Holladay, J.D., Hu, J., King, D.L., Wang, Y.: An overview of hydrogen production technologies. Catal. Today **139**, 244–260 (2009)
Hindmarsh, A.C.: Serial Fortran Solvers for ODE Initial Value Problems. (2006) http://computation.llnl.gov/casc/odepack/odepack_home.html. Accessed Sept 2014
Jang, S.C., Yang, S.I., Oh, S.G., Choi, D.K.: Adsorption dynamics and effects of carbon to zeolite ratio of layered beds for multicomponent gas adsorption. Korean J. Chem. Eng. **28**, 583–590 (2011)
Jayaraman, A., Hernández-Maldonado, A.J., Yang, R.T., Chinn, D., Munson, C.L., Mohr, D.H.: Clinoptilolites for nitrogen/methane separation. Chem. Eng. Sci. **59**, 2407–2417 (2004)
Joseck, F., Wang, M., Wu, Y.: Potential energy and greenhouse gas emission effects of hydrogen production from coke oven gas in U.S. steel mills. Int. J. Hydrogen Energy **33**, 1445–1454 (2008)
Karger, J., Ruthven, D.M.: Diffusion in Zeolites and Other Microporous Solids. Wiley, New York (1992)
Kearns, D.T., Webley, P.A.: Modelling and evaluation of dual-reflux pressure swing adsorption cycles: part I. Mathematical models. Chem. Eng. Sci. **61**, 7223–7233 (2006)
Kikkinides, E.S., Yang, R.T., Cho, S.H.: Concentration and recovery of CO_2 from flue gas by pressure swing adsorption. Ind. Eng. Chem. Res. **32**, 2714–2720 (1993)
Lopes, F.V.S., Grande, C.A., Ribeiro, A.M., Vilar, V.J.P., Loureiro, J.M., Rodrigues, A.E.: Effect of ion exchange on the adsorption of steam methane reforming off-gases on zeolite 13X. J. Chem. Eng. Data **55**, 184 (2010)
Lopes, F.V.S., Grande, C.A., Rodrigues, A.E.: Activated carbon for hydrogen purification by pressure swing adsorption: multicomponent breakthrough curves and PSA performance. Chem. Eng. Sci. **66**, 303–317 (2011)
Mofarahi, M., Shokroo, E.J.: Comparison of two pressure swing adsorption processes for air separation using zeolite 5A and zeolite 13X. Pet. Coal **55**, 216–225 (2013)
Park, J.H., Kim, J.N., Cho, S.H.: Performance analysis of four-bed H_2 PSA process using layered beds. AIChE J. **46**, 790–802 (2000)
Ribeiro, A.M., Grande, C.A., Lopes, F.V.S., Loureiro, J.M., Rodrigues, A.E.: Four beds pressure swing adsorption for hydrogen purification: case of humid feed and activated carbon beds. AIChE J. **55**, 2292–2302 (2009)
Riis, T., Hagen, E.F., Vie, P.J.S., Ulleberg, Ø.: Hydrogen Production R&D: Priorities and Gaps. IEA Publications, Paris (2006)
Ruthven, D.M.: Principles of Adsorption and Adsorption Processes. Wiley, New York (1984)
Ruthven, D.M., Farooq, S., Knaebel, K.S.: Pressure Swing Adsorption. VCH Publishers, New York (1994)
Saha, D., Bao, Z., Jia, F., Deng, S.: Adsorption of CO_2, CH_4, N_2O, and N_2 on MOF-5, MOF-177, and zeolite 5A. Environ. Sci. Technol. **44**, 1820–1826 (2010)
Sircar, S., Kumar, R.: Adiabatic adsorption of bulk binary gas mixtures: analysis by constant pattern model. Ind. Eng. Chem. Process Des. Dev. **22**, 271–280 (1983)
Sircar, S., Waldron, W.E., Rao, M.B., Anand, M.: Hydrogen production by hybrid SMR–PSA–SSF membrane system. Sep. Purif. Technol. **17**, 11–20 (1999)
Tomita, T., Sakamoto, T., Ohkamo, U., Suzuki, M.: Proceedings of the Second Engineering Foundation Conference on Fundamentals of Adsorption, Liapis, A.I. (ed). (Engineering Foundation, Nueva York, 1987)
Waldron, W.E., Sircar, S.: Parametric study of a pressure swing adsorption process. Adsorption **6**, 179–188 (2000)
Wankat, P.C.: Rate-Controlled Separations. Blackie Academic and Professional, London (1994)
Yang, R.T.: Gas Separation by Adsorption Processes. Imperial College Press, London (1997)
Yang, R.T.: Adsorbents: Fundamentals and Applications. Wiley, New Jersey (2003)
Yang, J., Lee, C.H., Chang, J.W.: Separation of hydrogen mixtures by a two-bed pressure swing adsorption process using zeolite 5A. Ind. Eng. Chem. Res. **36**, 2789–2798 (1997)
Zhou, L., Lu, C.Z., Bian, S.J., Zhou, Y.P.: Pure hydrogen from the dry gas of refineries via a novel pressure swing adsorption process. Ind. Eng. Chem. Res. **41**, 5290–5297 (2002)